Journal of Advances in Modeling Earth Systems

Supporting Information for

Sensitivity of the Atlantic Meridional Overturning Circulation to Model Resolution in CMIP6 HighResMIP Simulations and Implications for Future Changes

Malcolm J. Roberts[1], Laura C. Jackson[1], Christopher D. Roberts[2], Virna Meccia[3], David Docquier[4], Torben Koenigk[4], Pablo Ortega[5], Eduardo Moreno-Chamarro[5], Alessio Bellucci[6], Andrew Coward[7], Sybren Drijfhout[8], Eleftheria Exarchou[5], Oliver Gutjahr[9], Helene Hewitt[1], Doroteaciro Iovino[6], Katja Lohmann[9], Dian Putrasahan[9], Reinhard Schiemann[10], Jon Seddon[1], Laurent Terray[11], Xiaobiao Xu[12], Qiuying Zhang[13,14], Ping Chang[13,14], Stephen G. Yeager[15,14], Frederic S. Castruccio[15,14], Shaoqing Zhang[16,14], Lixin Wu[16,14]

[1] Met Office, Exeter EX1 3PB, U.K. [2] European Centre for Medium Range Weather Forecasting (ECMWF), Reading, U.K. [3] Istituto di Scienze dell'Atmosfera e del Clima (CNR-ISAC), Bologna, Italy [4] Rossby Centre, Swedish Meteorological and Hydrological Institute (SMHI), Norrköping, Sweden, [5] Barcelona Supercomputing Center – Centro Nacional de Supercomputación (BSC), Barcelona, Spain. [6] Fondazione Centro Euro-Mediterraneo sui Cambiamenti Climatici (CMCC), Bologna, Italy. [7] National Oceanography Centre, Southampton, U. K. [8] Koninklijk Nederlands Meteorologisch Instituut (KNMI), De Bilt, The Netherlands. [9] Max Planck Institute for Meteorology (MPI-M), Hamburg, Germany. [10] National Centre for Atmospheric Science (NCAS), University of Reading, Reading, U.K. [11] CECI, Université de Toulouse, CERFACS/CNRS, Toulouse, France. [12] Center for Ocean-Atmospheric Prediction Studies (COAPS)/FSU, Tallahassee, USA. [13] Texas A&M University, College Station, USA. [14] International Laboratory for High Resolution Earth System Prediction (iHESP), College Station, USA. [15] National Center for Atmospheric Research (NCAR), Boulder, USA. [16] Qingdao National Laboratory for Marine Science (QNLM), Qingdao, China.

Contents of this file

Introduction

This material is additional analysis that complements the main manuscript with some additional diagnostics and insight.

Text S1. AMOC latitudinal coherence

Additional insight into the how changes in the AMOC are propagated across latitudes.

The strength of the link between AMOC variations at different latitudes (Bingham et al, 2007) is central to disentangling the role of Labrador Sea waters on the AMOC, as well as to determine if the RAPID observations at 26.5°N are representative of the large-scale AMOC streamfunction. Previous studies have provided conflicting conclusions, suggesting both a strong link (e.g., Bailey et al, 2005; Böning et al., 2006; Eden & Willebrand, 2001; Kwon & Frankignoul, 2014; Saha et al., 2014; Yeager & Danabasoglu, 2014) and a weak or no link at all between AMOC changes at subpolar and subtropical latitudes (e.g., Li & Lozier, 2018; Li et al., 2019; Lozier et al., 2019; Polo et al, 2014; Zhao & Johns, 2014). We assess whether this link is sensitive to model resolution, ocean model family, or both in the 1950-control simulations on interannual timescales.

Only the CMCC-CM2 models exhibit a strong in-phase cross-latitudinal coherence in their AMOC variations, with synchronous changes between 60°N and the Equator for both model resolutions (Fig. S1). In the HadGEM3-GC31 simulations, increasing the atmospheric resolution while keeping the eddy-permitting resolution in the ocean (MM to HM versions) enhances the latitudinal coherence of the AMOC, suggesting that the atmosphere also plays a role in the latitudinal propagation of AMOC anomalies; however, cross-latitudinal coherence decreases when the oceanic resolution is increased as well (HH), which implies that it is sensitive to both atmospheric and oceanic configurations, and how they interact with each other. Most of the other models show a weak cross-latitudinal coherence in their AMOC variations between subpolar regions and further south, regardless of their resolution, in agreement with the latest evidence (Li et al., 2019; Lozier et al., 2019).

This lack of meridional coherence between subpolar and subtropical regimes in coupled climate models is consistent with the results of (Xu et al. 2019), in which they examined the correlation between the AMOC variability at specific latitudes and the basin-wide averaged AMOC variability in 44 CMIP5 historical runs and found that the correlation is lower in the subpolar region (45-60°N) than further south. The meridional heat transport anomalies inferred from observations (Kelly et al. 2014) and the AMOC variability based on an eddying ocean simulation (Xu et al. 2014) also suggested that the interannual variability of the AMOC transport is coherent for a latitude range south of 35-40°N, but not to the subpolar region further north.

Correlation coefficients tend to be statistically significant only 1 year before and after the zero-lag value in most of the models, which suggests a weak temporal persistence of the

AMOC anomalies on subdecadal to multidecadal time scales. This may also suggest that the 100 years of control-1950 simulation may not be sufficient to properly sample the model variability.

Text S2. AMOC overturning in V(θ,S)

Additional insight into the properties of the water masses in the AMOC.

Figure S2 shows the modeled V(θ,S) (see main text) across the subtropical North Atlantic at 26.5°N for 17 hist-1950 simulations shown in Table S2, along with the results from an eddying Atlantic simulation (bottom right) that has been shown to represent well the structure of the AMOC and subtropical gyre (Xu et al. 2016) – note the discrete distributions here due to the 1/12° HYCOM isopycnic vertical coordinate model. For this reference model, one can identify: i) the northward-flowing warm near surface water (>25ºC); ii) both northward and southward flowing thermocline (sometimes also termed eighteen degree water) and the Antarctic Intermediate Water (AAIW) above 36.64 kg/m^3, iii) the southward-flowing North Atlantic Deep Water (NADW, 36.64-37.12 kg/m^3), and iv) the northward-flowing Antarctic Bottom Water (AABW) below 37.12 kg/m^3. Note the northward-following component of thermocline water and AAIW in the western boundary are noticeably fresher and colder than the returning flow in the interior, implying that the positive evaporation over precipitation and upward air-sea heat flux in the subtropical North Atlantic (see Xu et al., 2016 for more discussion).

The hist-1950 simulations capture the overall water mass structure of the meridional transport reasonably well. Many simulations also capture that, in thermocline water and AAIW, the northward component of the subtropical gyre is slightly colder and fresher than the southward counterpart. This subtle difference is clearly better represented in the higher horizontal resolution simulation for all model cases (note the CMCC-CM2 and MPI-ESM1-2 models exhibit significantly wider salinity range than other models, probably in part due to the coarser vertical resolution used - see Table 1). However, nearly all simulations show a cold bias for the near-surface water (see also Fig. 3) and most simulations show an excessive presence of Mediterranean outflow water (at the salinity peak, see also Fig. 3 near 900 m). It is also notable that the difference in V(θ,S) due to different horizontal resolutions is generally far smaller than that between different models, implying that the time-mean state of the AMOC and the water masses is more sensitive to the combined effect of other model configuration details (e.g., the atmosphere, sea ice, vertical resolution, viscosity and/or eddy parameters in the ocean, etc.) than the horizontal resolution alone.
V(θ,S) can also be integrated along isotherms, isohalines and isopycnals to yield the overturning streamfunction with respect to temperature, salinity and density; and the overturning in density space is discussed in Fig. 6a.

Text S3. Sub-annual variability

In order to explore the sub-annual variability, the mean and standard deviation of the monthly values of AMOC at 26.5°N were calculated (Table S2) over the hist-1950 runs, that is for the period 2004-2015. All the available ensemble members were considered in the computation. The mean value of the observed monthly AMOC at 26.5°N for the period 2004-2017 is 16.96 Sv and its standard deviation is 3.29 Sv. As for the annual values, the modelled monthly mean AMOC is, in general, underestimated with respect to the observations. However, HadGEM3-GC31 in its highest resolutions (HM and HH), CMCC-CM2 in its both configurations and MPI-ESM1-2-HR simulate higher mean values than the observed one. Therefore, the multi-model mean results in 16.25 Sv, a slightly lower than RAPID mean AMOC. The monthly standard deviations range between 2.41 and 4.36 Sv. Models simulate a higher variability with the increasing ocean resolution (HadGEM3-GC31, ECMWF-IFS, CNRM-CM6-1 and EC-Earth3P). The multi-model standard deviation results in 3.11 Sv which is very close to the observed value. This suggests that, even though the inter-annual variability of the AMOC is underestimated in the models as was also found in Roberts et al., (2014), the sub-annual variability seems to be better captured.

References

Bailey, D. A., Rhines, P. B., & Häkkinen, S. (2005). Formation and pathways of North Atlantic Deep Water in a coupled ice–ocean model of the Arctic–North Atlantic Oceans. *Climate Dynamics*, *25*(5), 497–516. https://doi.org/10.1007/s00382-005-0050-3

Bingham, R. J., Hughes, C. W., Roussenov, V., & Williams, R. G. (2007). Meridional coherence of the North Atlantic meridional overturning circulation. *Geophysical Research Letters*, *34*(23). https://doi.org/10.1029/2007GL031731

Böning, C. W., Scheinert, M., Dengg, J., Biastoch, A., & Funk, A. (2006). Decadal variability of subpolar gyre transport and its reverberation in the North Atlantic overturning. *Geophysical Research Letters*, *33*(21). https://doi.org/10.1029/2006GL026906

Eden, C., & Willebrand, J. (2001). Mechanism of Interannual to Decadal Variability of the North Atlantic Circulation. *Journal of Climate*, *14*(10), 2266–2280. https://doi.org/10.1175/1520-0442(2001)014<2266:MOITDV>2.0.CO;2

Kelly, K. A., Thompson, L., & Lyman, J. (2014). The Coherence and Impact of Meridional Heat Transport Anomalies in the Atlantic Ocean Inferred from Observations. *Journal of Climate*, *27*(4), 1469–1487. https://doi.org/10.1175/JCLI-D-12-00131.1

Kwon, Y.-O., & Frankignoul, C. (2014). Mechanisms of Multidecadal Atlantic Meridional Overturning Circulation Variability Diagnosed in Depth versus Density Space. *Journal of Climate*, *27*(24), 9359–9376. https://doi.org/10.1175/JCLI-D-14-00228.1

Li, F., & Lozier, M. S. (2018). On the Linkage between Labrador Sea Water Volume and

Overturning Circulation in the Labrador Sea: A Case Study on Proxies. *Journal of Climate*, *31*(13), 5225–5241. https://doi.org/10.1175/JCLI-D-17-0692.1

Li, F., Lozier, M. S., Danabasoglu, G., Holliday, N. P., Kwon, Y.-O., Romanou, A., … Zhang, R. (2019). Local and Downstream Relationships between Labrador Sea Water Volume and North Atlantic Meridional Overturning Circulation Variability. *Journal of Climate*, *32*(13), 3883–3898. https://doi.org/10.1175/JCLI-D-18-0735.1

Lozier, M. S., Li, F., Bacon, S., Bahr, F., Bower, A. S., Cunningham, S. A., … Zhao, J. (2019). A sea change in our view of overturning in the subpolar North Atlantic. *Science*, *363*(6426), 516 LP – 521. https://doi.org/10.1126/science.aau6592

Polo, I., Robson, J., Sutton, R., & Balmaseda, M. A. (2014). The Importance of Wind and Buoyancy Forcing for the Boundary Density Variations and the Geostrophic Component of the AMOC at 26°N. *Journal of Physical Oceanography*, *44*(9), 2387–2408. https://doi.org/10.1175/JPO-D-13-0264.1

Roberts, C. D., Jackson, L., & McNeall, D. (2014). Is the 2004–2012 reduction of the Atlantic meridional overturning circulation significant? *Geophysical Research Letters*, *41*(9), 3204–3210. https://doi.org/10.1002/2014GL059473

Saha, S., Moorthi, S., Wu, X., Wang, J., Nadiga, S., Tripp, P., … Becker, E. (2014). The NCEP Climate Forecast System Version 2. *Journal of Climate*, *27*(6), 2185–2208. https://doi.org/10.1175/JCLI-D-12-00823.1

Xu, X., Chassignet, E. P., Johns, W. E., Schmitz Jr, W. J., & Metzger, E. J. (2014). Intraseasonal to interannual variability of the Atlantic meridional overturning circulation from eddy-resolving simulations and observations. *Journal of Geophysical Research: Oceans*, *119*(8), 5140–5159. https://doi.org/10.1002/2014JC009994

Xu, X., Chassignet, E. P., & Wang, F. (2019). On the variability of the Atlantic meridional overturning circulation transports in coupled CMIP5 simulations. *Climate Dynamics*, *52*(11), 6511–6531. https://doi.org/10.1007/s00382-018-4529-0

Xu, X., Rhines, P. B., & Chassignet, E. P. (2016). Temperature–Salinity Structure of the North Atlantic Circulation and Associated Heat and Freshwater Transports. *Journal of Climate*, *29*(21), 7723–7742. https://doi.org/10.1175/JCLI-D-15-0798.1

Yeager, S., & Danabasoglu, G. (2014). The Origins of Late-Twentieth-Century Variations in the Large-Scale North Atlantic Circulation. *Journal of Climate*, *27*(9), 3222–3247. https://doi.org/10.1175/JCLI-D-13-00125.1

Zhao, J., & Johns, W. (2014). Wind-forced interannual variability of the Atlantic Meridional Overturning Circulation at 26.5°N. *Journal of Geophysical Research: Oceans*, *119*(4), 2403–2419. https://doi.org/10.1002/2013JC009407

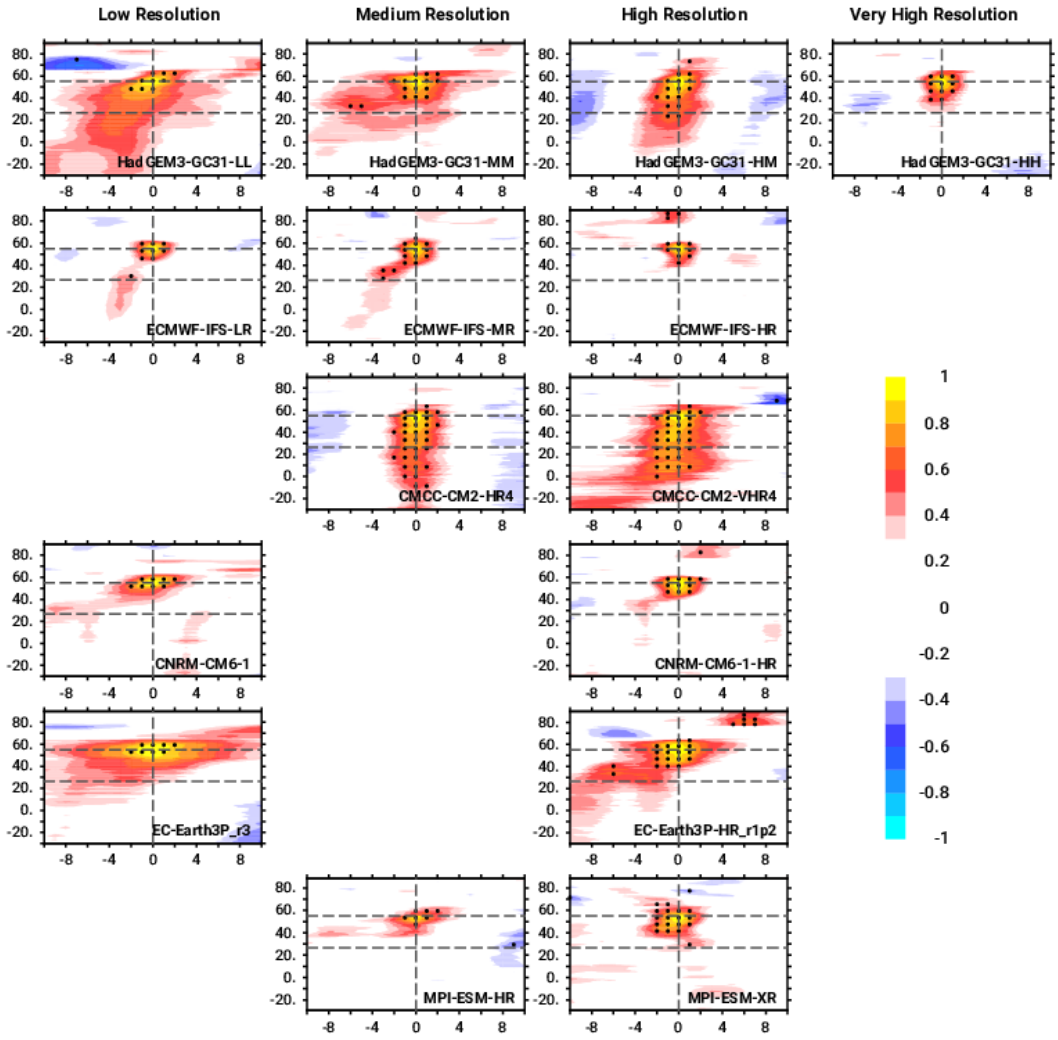

Figure S1. Cross-correlation profiles between the AMOC intensity at 55°N and any other latitude at the density level of the strongest AMOC intensity at 55°N (between 36.5 and 37 kg/m^3 in most of the models). Stippling masks values which are statistically significant at the 5 % level, accounting for autocorrelation and effective sample size in the time series. The AMOC at 55°N leads in positive years (horizontal axis), and vice versa. Time series are first detrended with a 2nd degree polynomial, to remove the effect of long-term model drifts, and then smoothed with a 3-year running mean, to filter out the noise of the year-to-year variations. Horizontal dashed lines are at 55°N and 26.5°N (i.e., RAPID-MOCHA latitude).

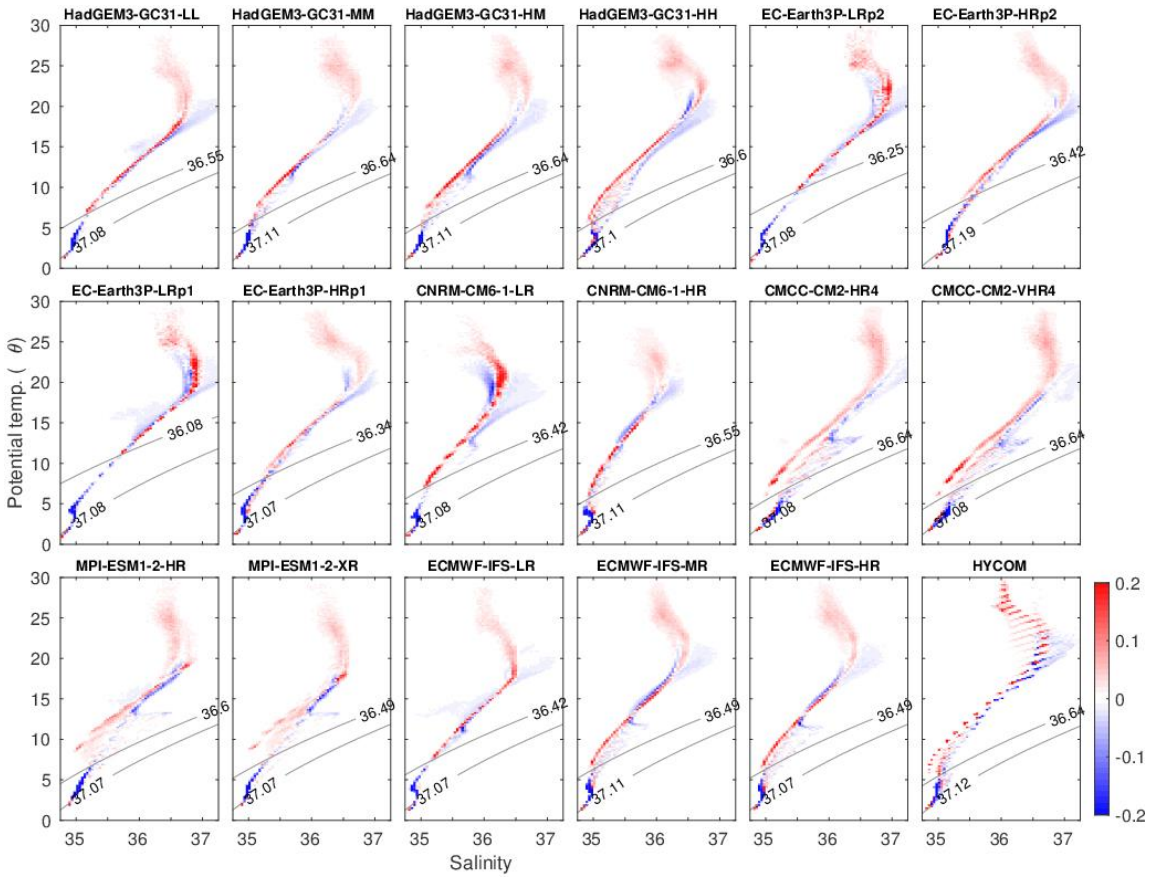

Figure S2. Meridional volume transport (in Sv) across 26.5°N in the North Atlantic projected on potential temperature - salinity (θ-S) plane with a $\Delta\theta \times \Delta S$ box of 0.2°Cx0.04psu. The results are based on monthly means hist-1950 simulations for 1979-2014. For a comparison, the last panel is results from a 1/12° Atlantic simulation in Xu et al (2016) in which the water mass structure of the AMOC and subtropical gyre is shown to be consistent with the observations. The two density surfaces in each panel denote the modeled interfaces 1) between the northward-flowing upper layer water and southward-flowing NADW (thus the AMOC), and 2) between the southward-flowing NADW and the northward-flowing Antarctic Bottom water (AABW) near the bottom.

Models/RapidMoc parameter	fc_minlon, fc_maxlon (deg E)	wbw_maxlon (deg E)	int_maxlon (deg E)
HadGEM3-GC31-LL	-81.0, -74.0	-73.0	-10.0
HadGEM3-GC31-MM	-81.0, -78.2	-75.5	-10.0
HadGEM3-GC31-HM	-81.0, -78.2	-75.5	-10.0
HadGEM3-GC31-HH	-81.0, -77.1	-76.1	-10.0
ECMWF-IFS-LR	-81.0, -74.5	-73.5	-10.0
ECMWF-IFS-MR	-81.0, -78.2	-75.5	-10.0
ECMWF-IFS-HR	-81.0, -78.2	-75.5	-10.0
CNRM-CM6-1	-81.0, -77.5	-73.5	-10.0
CNRM-CM6-1-HR	-81.0, -78.2	-75.5	-10.0
EC-Earth3P	-81.0, -77.5	-73.5	-10.0
EC-Earth3P-HR	-81.0, -78.2	-75.5	-10.0
CMCC-CM2-HR4	-81.0, -78.2	-75.5	-10.0
CMCC-CM2-VHR4	-81.0, -78.2	-75.5	-10.0
MPI-ESM2.1-HR	-81.0, -75.6	-75.0	-8.0
MPI-ESM2.1-XR	-81.0, -75.6	-75.0	-8.0
CESM1-3-LL	-80.3, -76.5	-75.5	-13.0
CESM1-3-HH	-80.3, -77.3	-76.8	-13.0
All models	Ekman_depth=50 georef_level=4750	ek_profile_type=linear	reference_salinity=35.17

Table S1. Option values input to the RapidMoc code to calculate the AMOC components at 26.5°N.

Models/RAPID	Mean	St Dev	# of members
HadGEM3-GC31-LL	15.09	2.85	8
HadGEM3-GC31-MM	16.80	3.41	1
HadGEM3-GC31-HM	18.38	3.42	3
HadGEM3-GC31-HH	20.66	3.49	1
ECMWF-IFS-LR	9.96	2.41	8
ECMWF-IFS-MR	13.93	2.85	3
ECMWF-IFS-HR	14.27	2.90	6
CNRM-CM6-1	16.22	2.81	1
CNRM-CM6-1-HR	16.06	3.87	1
EC-Earth3P	13.27	2.65	3
EC-Earth3P-HR	14.06	2.97	3
EC-Earth3P*	13.15	2.74	4
EC-Earth3P-HR*	14.02	2.99	4
CMCC-CM2-HR4	23.26	2.63	1
CMCC-CM2-VHR4	24.45	2.61	1
MPI-ESM2.1-HR	17.66	4.36	1
MPI-ESM2.1-XR	15.13	4.03	1
CESM1-3-LL			1
CESM1-3-HH			1
RAPID	16.96	3.29	

Table S2. Mean and standard deviation of monthly AMOC index for model/resolution of the hist-1950 runs and RAPID data. All the available ensemble members (last column) are included in the computation. Results for EC-Earth3P* and EC-Earth3P-HR* include the member r1i1p1f1.